ENGINEERING TRANSACTIONS • *Engng. Trans.* • 40, 3, 343–362, 1992
Polish Academy of Sciences • Institute of Fundamental Technological Research

STRENGTH AND FRACTURE ANALYSIS OF BRITTLE PHOTOELASTIC MATERIAL
STATIC AND DYNAMIC TESTS

L. KRUSZKA, W. K. NOWACKI and M. WOLNA (WARSZAWA)

Results of static and dynamic uniaxial compression tests on brittle transparent model material are presented. Multiple static experiments were made with the use of ultrasonic measurements, acoustic emission, photoelasticity and photographic registration of changes in the studied specimens. In this way comprehensive information on the mechanics of defects and fracture of the material was collected. In the dynamic investigations a standard Hopkinson bar device was used. Static and dynamic characteristics were compared, short-term strengths and mechanisms of cracking and fracture were studied, taking into account slenderness of testpieces.

1. INTRODUCTION

Brittle photoelastic materials are frequently used to investigate stress and strain states in monolithic engineering structures and their members, especially at collapse. Increasing interest is also directed towards application of these materials to study generation of cracks in structures or models made of real materials.

Photoelastic coating method is used for the purpose. Brittle photoelastic materials are also used to study the behaviour of rocks. Fragments of mining pits are modelled or photoelastic materials are bonded on the specimens of actual rock material. Cracking processes together with propagation of induced cracks can be modelled. Brittle fracture is also investigated in the boundary value problems.

The main aim of this paper is to examine the static and dynamic behaviour of a brittle photoelastic material made of local components. The purpose is not only to better understand the properties of the material, but also to acquire information useful for complete (nonstructural) modelling of specific engineering structures.

The whole analysis should be completed with the comparison of properties of the tested material with the properties of actual brittle materials under consideration such as rocks and concretes. This problem will be dealt with in a separate paper.

In this paper the test results from long-term compression (low strain rates of $\dot{\varepsilon} = 3 - 14 \cdot 10^{-5}\,s^{-1}$) are compared with those from the dynamic compression (high strain rates of the order of $10^3\,s^{-1}$). Four slenderness ratios of uniaxial compression cylindrical specimens were used.

Three types of experiments were planned:

- preliminary tests: nondestructive ones based on ultrasonic measurements,
- main ones: destructive tests in both static and dynamic regimes,
- auxiliary: static tests based on the acoustic emission, photoelasticity and photographic registration of deformation process in specimens under study.

Thus a large amount of information can be collected to describe processes of crack propagation and fracture mechanisms. Modelling of brittle fracture was attempted with the use of brittle model material without the necessity of an artificial crack. Few experiments of this type has been reported in the literature. Studies described in this paper comprise the necessary tools and programmes of some preliminary investigations in the field of fracture mechanics. The obtained results should therefore be treated as having mainly a qualitative character.

2. Preparation of modelling material

Locally available materials were used to make the photoelastic material: epoxy resin Epidian 2 and distilled rosin. Method of preparation was described in [1]. A series of cylindrical specimens were made with the diameter of $d_0 \simeq 17\,mm$ and the heights $h_0 = 0.5d_0;\ d_0;\ 1.5d_0;\ 2d_0$. Specimens were formed in moulds made of silicone rubber Polastosil M56 networked at room temperature with a 5% addition of catalizer OL-1. Due to flexibility of moulds, practically no residual stresses were generated in the specimens after pouring. To obtain smooth surface and parallel bases, cylindrical specimens were machined by turning.

Average specific weight of the material was $\gamma = 11.2\,kN/m^3$, average Brinell's hardness amounted to $H_B = 23.2$.

The following designations of specimens were used:

- slenderness $s = 0.5;\ 1.0;\ 1.5;\ 2.0$ by means of letters A, B, C, D,
- consecutive casts: I – V,
- consecutive numbers of specimens with the same slenderness 1 – 8.

3. Nondestructive tests

Prior to the basic experiments some nondestructive tests were made in order to select specimens suitable for further investigations and to determine material constants (wave elastometry). Ultrasonic technique was used. Retardations of impulses (echo of specimen's bottom) were measured with the help of a defectoscope supplied with a transmitter of 4 MHz frequency. Velocities of ultrasonic waves were found to be almost uniform (admissible scatter was not exceeded) so the tested material was considered to be physically homogeneous. The method of ultrasonic elastometry made it possible to determine the following average values of material constants:

- propagation velocities of elastic waves; for longitudinal waves $c_L = 2480\,\mathrm{m/s}$, for transverse waves $c_T = 1096\,\mathrm{m/s}$,
- Lamé's constants: $\lambda = 4410\,\mathrm{MPa}$, $\mu = 1410\,\mathrm{MPa}$,
- Young's modulus $E = 3770\,\mathrm{MPa}$, bulk modulus $K = 5240\,\mathrm{MPa}$,
- Poisson's ratio $\nu = 0.38$.

Apart from ultrasonic verification, residual stresses were checked. Photoelastic measurements were taken in a circularly polarised light, whereas the studied specimens were sunk in an immersion fluid. Although intensive cooling was applied during machining of testpieces, some permanent residual stresses were found to be present. Such a sensitive measuring method as photoelasticity showed clearly those residual stresses. However, those small stresses did not affect the stress state generated in compression in any appreciable manner.

4. Destructive and complementary tests

Destructive tests constituted the main part of the investigations. Cylindrical specimens were subjected to uniaxial compression to failure under static and dynamic conditions.

4.1. Static tests

Static compression was realized in a mechanical testing machine with the constant velocity of its traverse $v_t = 0.07$ mm/min. Global strain rate in the deformation process was $\dot{\varepsilon} = v_t/h_0$. Diagrams of compressive force F versus displacement $\Delta h = h_0 - h$ (change in the distance between platens) were prepared. Global strains were measured as referred to the whole height of a specimen to provide preliminary conclusions of a rather qualitative character. Some drawbacks of this simple procedure are described in [2]. However, gauge measurements of local strains in the course of tests to failure are usually difficult, if at all possible, especially in the post-elastic range and close to the strain gauges whose bases are small but finite.

Displacements were measured with the use of an induction-type register of length changes. Two loading programmes were realized:

- up to the attainment of short-term strength, with no unloading,
- with four loading-full unloading cycles before the short-term strength was reached. In the first cycle (I) about 20 per cent of the maximum load F_c was applied (as an average for a given slenderness of specimens), in cycle II – 40 per cent, in cycle III – 60 per cent and in cycle IV – 80 per cent (Figs.1–4).

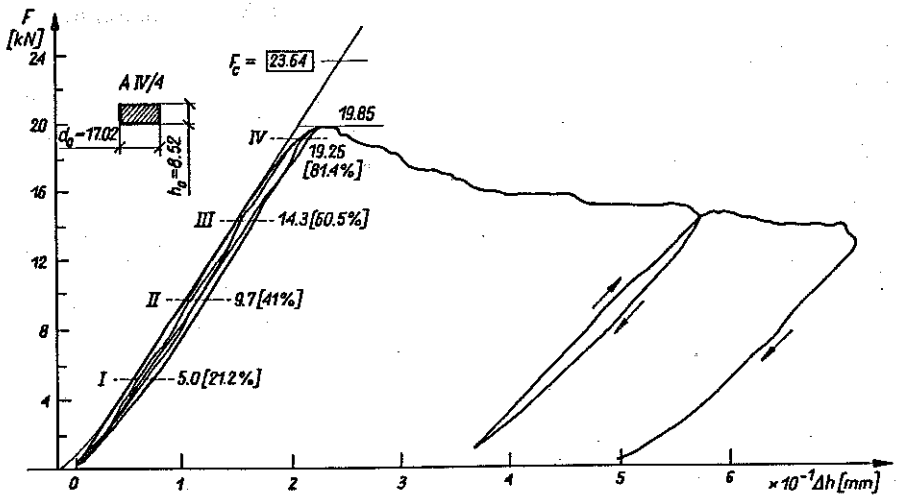

FIG. 1. Axial compressive force F vs. displacement Δh diagram with four (I–IV) cycles of loading-unloading; specimen AIV/4 ($s = 0.5$); F_c – average short-term strength from no-unloading tests for specimens with the slenderness $s = 0.5$.

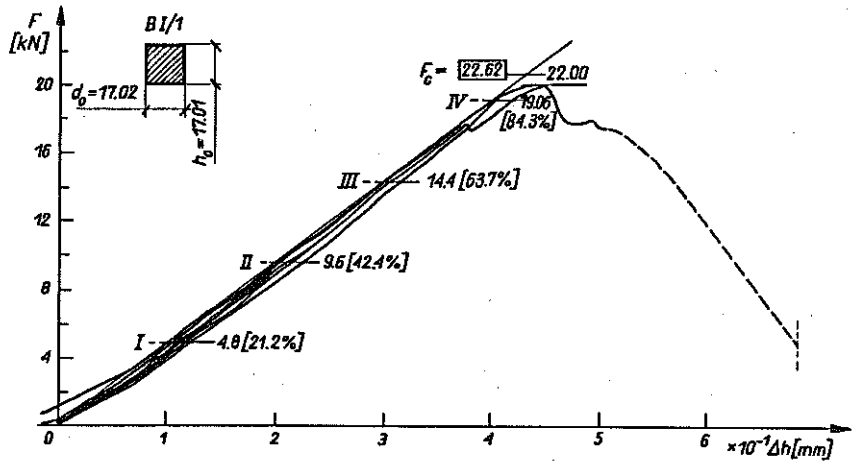

FIG. 2. Axial compressive force F vs. displacement Δh diagram with four (I–IV) cycles of loading-unloading; specimen BI/1 ($s = 1$); F_c – average short-term strength from no-unloading tests for specimens with the slenderness $s = 1$.

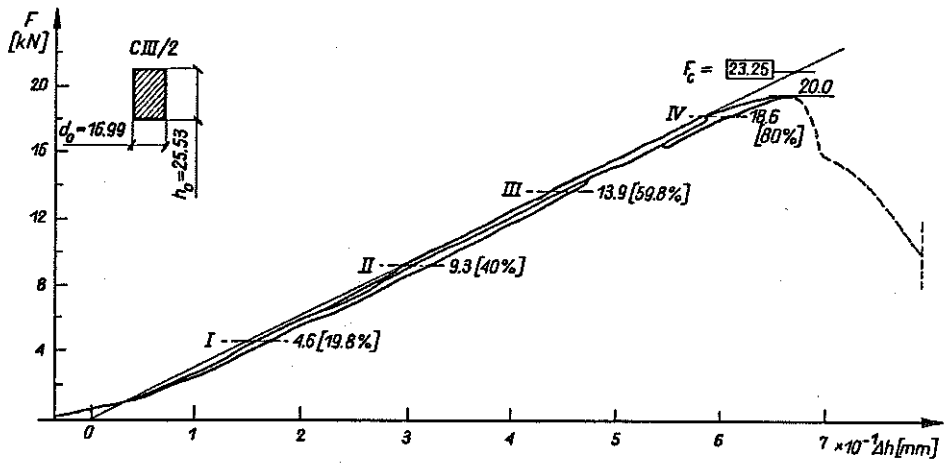

FIG. 3. Axial compressive force F vs. displacement Δh diagram with four (I–IV) cycles of loading-unloading; specimen CIII/2 ($s = 1.5$); F_c – average short-term strength from no-unloading tests for specimens with the slenderness $s = 1.5$.

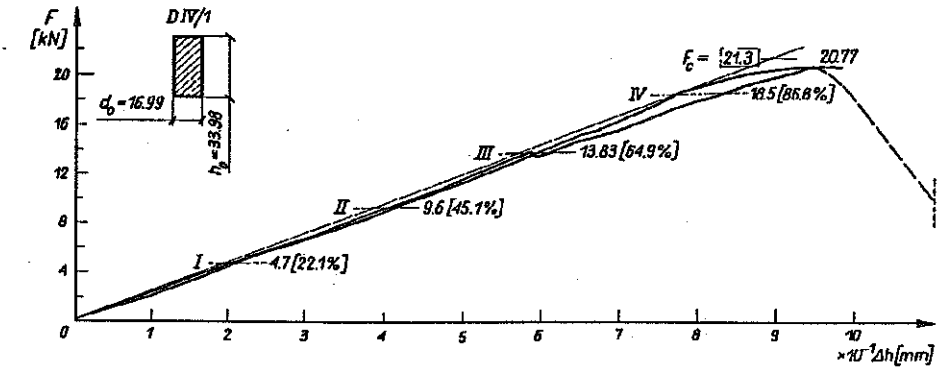

FIG. 4. Axial compressive force F vs. displacement Δh diagram with four (I–IV) cycles of loading-unloading; specimen DIV/1 ($s = 2$); F_c – average short-term strength from no-unloading tests for specimens with the slenderness $s = 2$.

Average nominal stresses $\sigma = F/A_0$ (A_0 – initial cross-section of a cylinder) as functions of global strain $\varepsilon = \Delta h/h_0$ for four slendernesses are shown in Fig.5. The results were obtained in the testing machine during the first

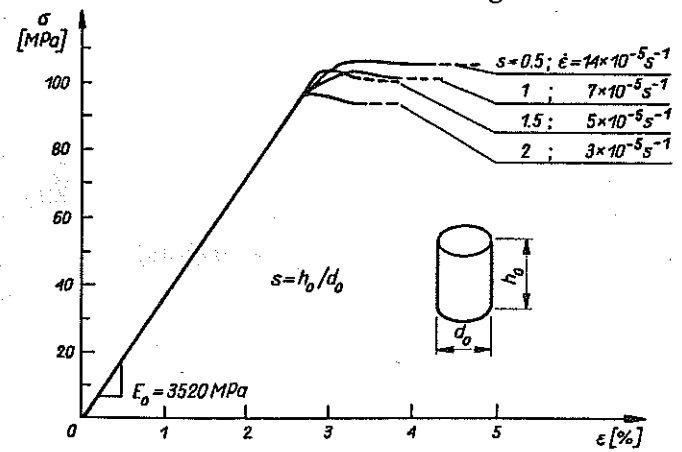

FIG. 5. Average nominal static stress σ vs. global strain ε for various slenderness of specimens; E_0 – average static Youn's modulus, $\dot{\varepsilon}$ – strain rate.

loading programme. Average static Young's modulus E_0 was found to be 3520 MPa. The presented curves do not contain their postcritical branches (softening characteristics) that largely depend on the type of failure. They will be shown later on. Along with the compression, deformation changes were registered photographically in the unpolarized and the circularly polarized sodium light. At an instant of compression programme at which plastic deformations appear on the matting surfaces of specimens, some

thin slip lines (Liiders – Hartman – Cherenkov lines) can be seen inclined at roughly 45° to the specimen axes (coinciding with the inclination of extremum shearing stresses). Dark regions of shear strains (plastic ones) can also be observed inside cylinders as shown in Fig.6.

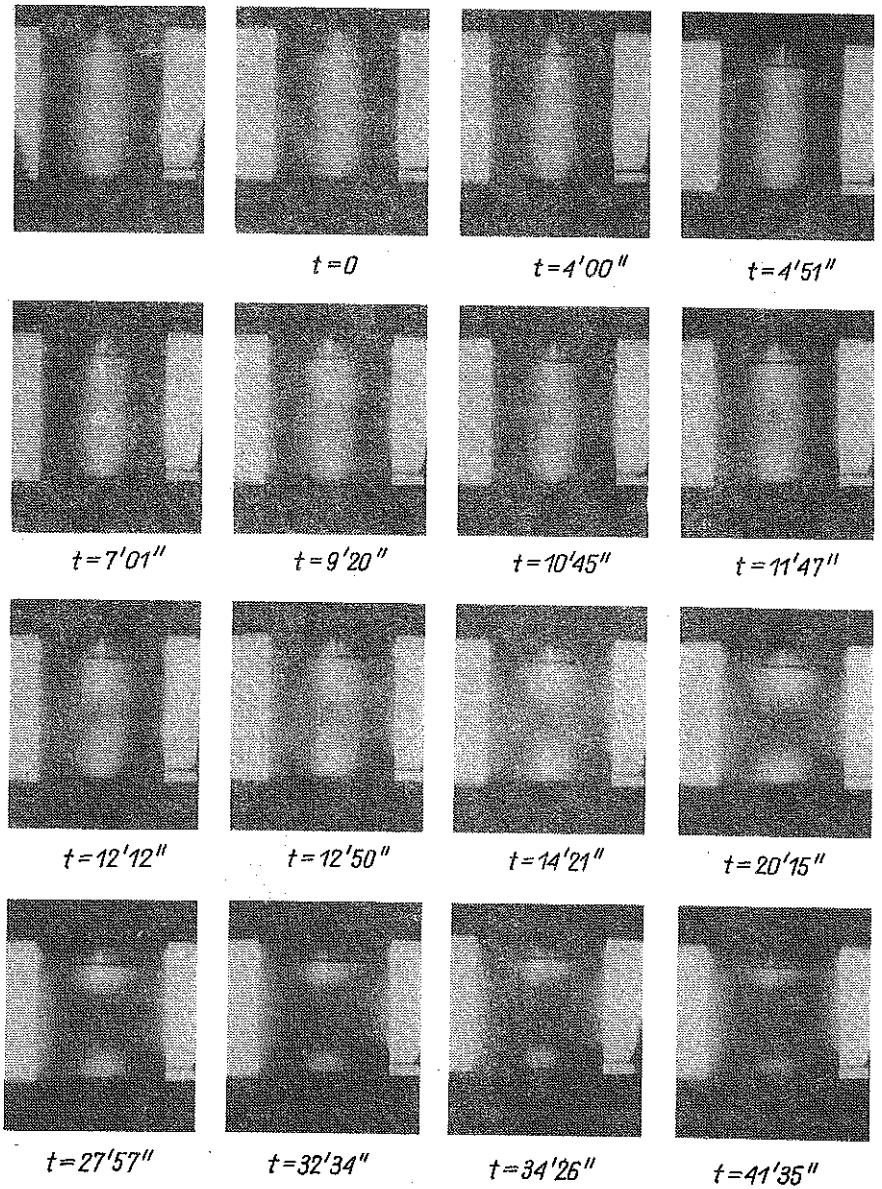

FIG. 6. Shear strain regions in specimen BII/3 ($s = 1$) for various instants.

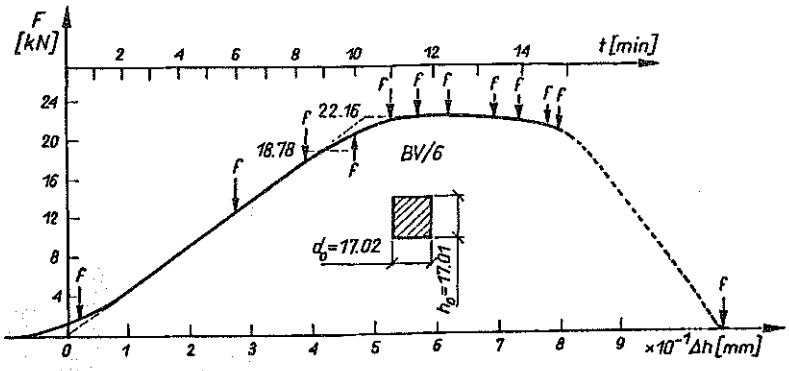

FIG. 7. Variability of compressive force in specimen BV/6.

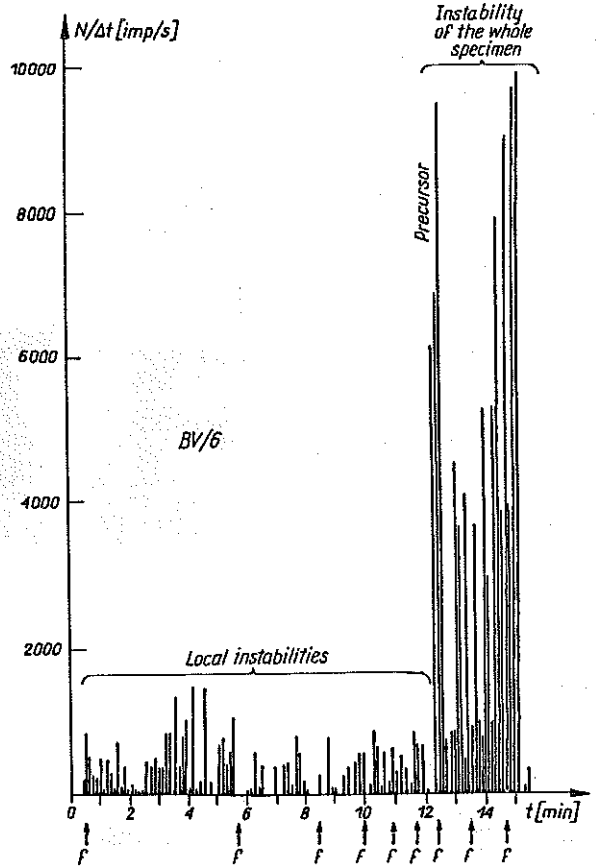

FIG. 8. Signal of acoustic emission $N/\Delta t$ (number of impulses per unit of time) during measurements of t in specimen BV/6.

Acoustic emission method was also employed to study the deformation process. Load-displacement relationship is shown in Fig.7. Symbols f correspond to the photographs – Fig.10. Number of acoustic impulses per unit of time $N/\Delta t$ is shown in Fig.8 and respective RMS (root mean squares) can be seen in Fig.9. The latter indicates an effective magnitude of voltage

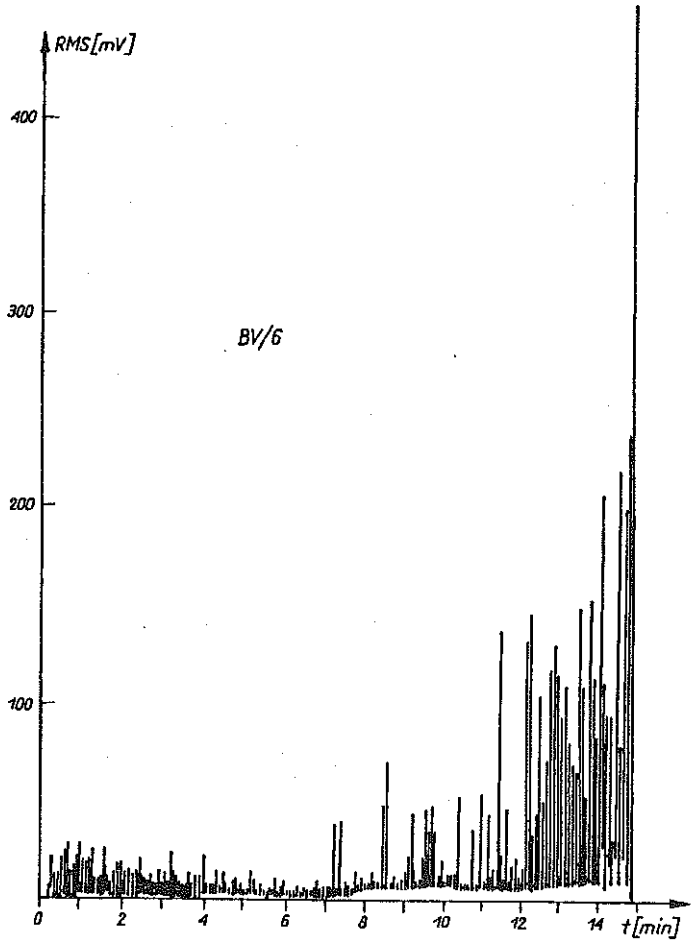

FIG. 9. Signal of acoustic emission RMS (root mean square) during measurements of t in specimen BV/6.

which is proportional to the amount of elastic energy stored in the material under compression. Results of auxiliary photographic studies for specimen BV/6 during its deformation process are shown in Fig.10.

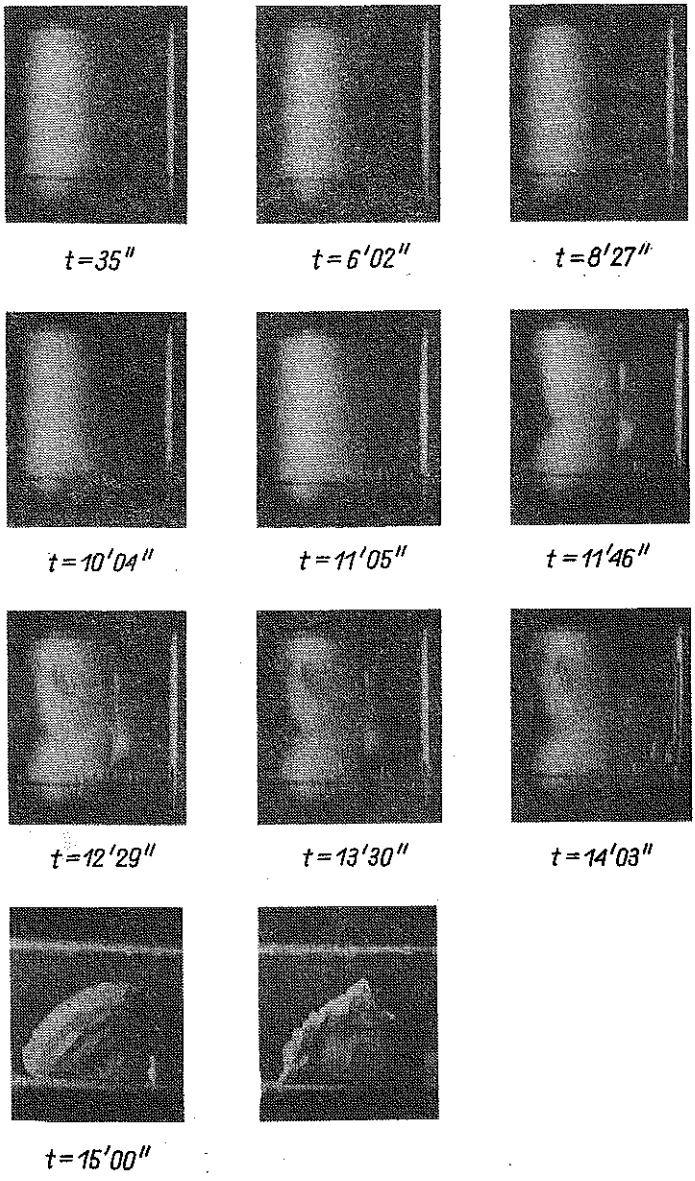

FIG. 10. Deformation and failure process of specimen BV/6.

To avoid excessive friction between specimens and platens silicone paste, graphite grease and molybdenum disulphide with an addition of kerosene were applied to the bases of cylinders. No appreciable differences between these three lubricants were found as to the load-displacement curves. In further tests silicone paste only was used.

4.2. Dynamic tests

The modified Hopkinson bar (see e.g. [3]) was used for dynamic tests. This technique was first devised to study plastic properties of metals at high strain rates. It has found broad applications also for the studies of dynamic behaviour of other materials such as plastics and brittle materials – in particular rocks and concretes [4–13]. This procedure makes it possible to observe the whole process of dynamic loading of a cylindrical specimen including an instant of fracture and subsequent fragmentation leading to the final destruction of the specimen. Cylindrical specimens with the diameters $d_0 \simeq 17$ mm and various height-to-diameter ratios were subjected to compressive action of 100 – 160 μs duration. Detailed description of testing stand and suitable experiments is given in [14].

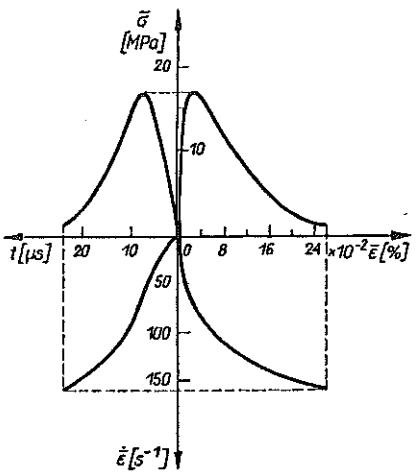

FIG. 11. Diagrams of $\sigma - \varepsilon$, $\sigma - t$, $\dot{\varepsilon} - t$, $\dot{\varepsilon} - \varepsilon$ for specimen CIII/1 ($s = 1.5$) under dynamic load.

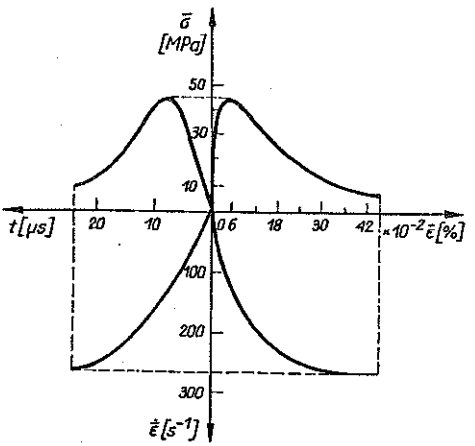

FIG. 12. Diagrams of $\sigma - \varepsilon$, $\sigma - t$, $\dot{\varepsilon} - t$, $\dot{\varepsilon} - \varepsilon$ for specimen CIII/3 ($s = 1.5$) under dynamic load.

Relevant results of dynamic tests are given for four selected specimens: C III/1, C III/3, DIV/2 and DVI/7 (Figs.11–14, respectively). The shown

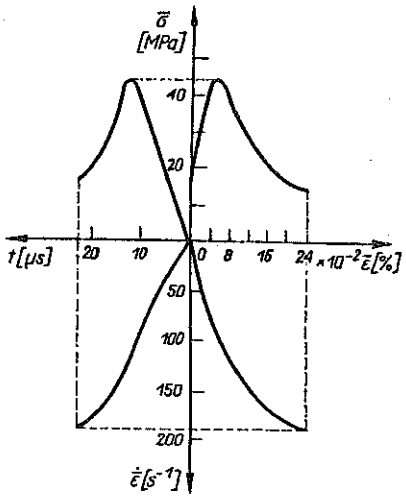

FIG. 13. Diagrams of $\sigma - \varepsilon$, $\sigma - t$, $\dot{\varepsilon} - t$, $\dot{\varepsilon} - \varepsilon$ for specimen DIV/2 ($s = 2$) under dynamic load.

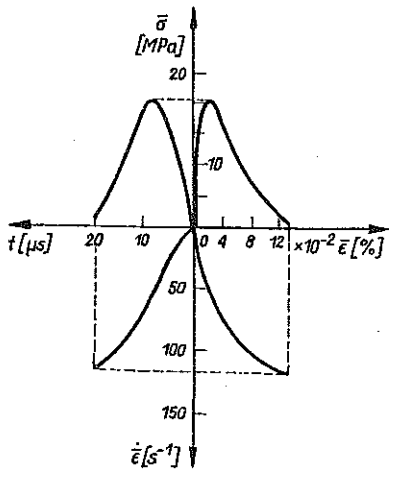

FIG. 14. Diagrams of $\sigma - \varepsilon$, $\sigma - t$, $\dot{\varepsilon} - t$, $\dot{\varepsilon} - \varepsilon$ for specimen DIV/7 ($s = 2$) under dynamic load.

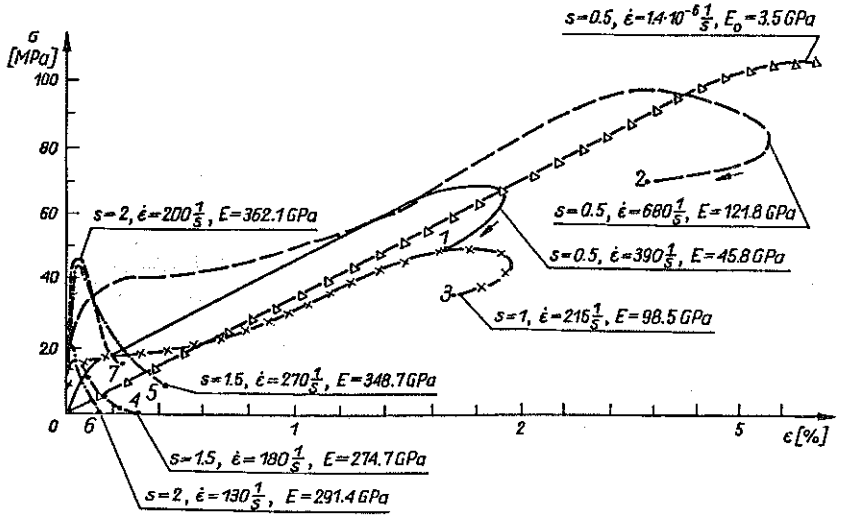

FIG. 15. Dynamic $\sigma - \varepsilon$ curves for specimens with various slendernesses and subjected to various strain rates $\dot{\varepsilon}$. E – dynamic Young's modulus. Statical $\sigma - \varepsilon$ curve for $s = 0.5$ is also shown (with triangles). Designations of specimens: 1 – AII/2, 2 – AV/6, 3 – BII/2, 4 – CIII/1, 5 – CIII/3, 6 – DVI/7, 7 – DVI/2.

curves comprise: stress-strain diagrams, stress and strain rate diagrams as functions of time and strain-strain rate relationships in terms of averaged values (dashes over symbols). Dynamic stress-strain curves are presented in Fig.15 for seven specimens with various slendernesses and subjected to various strain rates. Static curve for $s = 0.5$ is also shown. Considerable increase in dynamic Young's modulus can be observed. Dynamic unloading can be clearly seen in specimens with lower slendernesses ($s = 0.5$ and $s = 1.0$). The tested material is found to be strain-rate sensitive (compare for $s = 0.5$: $\dot{\varepsilon} = 1.4 \cdot 10^{-6}\,s^{-1}$, $390\,s^{-1}$, $680\,s^{-1}$). However, the largest stresses were those reached under static loading. Similar behaviour was found to apply to the epoxy resin specimens, Fig.16 [31].

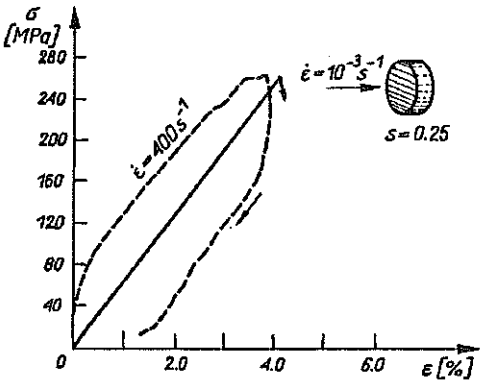

FIG. 16. Static and dynamic $\sigma - \varepsilon$ curves for a cylindrical epoxy resin specimen with the slenderness $s = 0.25$.

4.3. Degradation of a photoelastic material under various strain rates

Brittle materials are characterized by creation of microcracks upon loading followed by the desintegration of a testpiece. That is why a rigidity of a mechanical loading system plays an important role in the tests [15]. If a post-failure characteristic of a brittle material has larger slope than that of a loading system, a sudden desintegration of the material will occur.

Thus a considerable rigidity of the testing machine is advisable to enable accurate measurements of the material properties during the falling branch of the load-displacement curve and to obtain information on both ascending and descending branches of the process. Testing machines and Hopkinson bars used in this type of experiments are found to be rigid enough. Increas-

ing input of energy makes it possible to observe the whole failure process and particular stages of the fragmentation to be registered photographically, at least in static tests. Static and dynamic deformation processes are accompanied by the formation of microcracks followed by growth and accumulation of microdefects that result in the creation of one or more macrocracks and final destruction of the material. These processes have been found to be anisotropic phenomena that strongly depend on strain rates, geometry of specimens, and the existing friction between specimens and platens (contact forces). The following stages of the static as well as dynamic loading have been observed to take place – elastic behaviour, commencement of cracks degradation of the material and fragmentation (final failure).

Main advantage of the tested brittle material is its transparency and sensitivity to the effects of birefrengence. Unlike in nontransparent materials such as rocks and concretes, it enables an uninterrupted, continuous observation of the deformation process [16] which can be in static tests easily registered by photographic means. Moreover, an experimental analysis of stress and strain states is possible once the photelastic images are obtained.

As mentioned before, the boundary conditions at the interfaces of samples and platens of a testing machine are of particular importance. Friction between the tested material and platens and much larger stiffness of platens than of the samples cause serious disturbances in the uniaxial stress state and lead to the presence of shearing action as a result of lateral constraints – are important factor in the brittle fracture of materials. According to the Saint–Venant principle, it is not closer than at a distance of the specimen diameter that a way in which loading is applied ceases to influence appreciably the behaviour. That is why the testpiece heights amount to twice or three times the lateral dimensions [17–19]. For the slenderness ratio s larger than 2 the compressive stress state is considered to be practically homogeneous – at least prior to the appearance of the first crack. Effects of slenderness on the strength of specimens are discussed in [20] where some photographs of crack and failure modes are shown. In slender specimens ($s > 1$) faulting occurs in the form of single inclined shears. When $s = 1$, characteristic inverted cones are formed as a result of shear and axial splittings as well as slabbing. In short specimens ($s = 0.5$) numerous splits occur accompanied by surface spalling. All these deformation modes indicate the presence of contact friction. Classical longitudinal splitting, characteristic for brittle material under compression with negligible frictional resistance was not found to occur. Simlilar failure modes for the static compression of

brittle cylindrical testpieces have been described in the literature for rocks in [21–24] for concrete (also for biaxially compressed cubes) in [25], for mortars in [26], for hardened steel and cast iron in [27].

Additional knowledge of the course of failure of specimens under static load was gathered with the help of acoustic emission (AE) signals that carried information about discrete processes going on in the material in contrast to the load-displacement (or stress-strain) relationships that reflect generalized, continuous changes due to loading. According to the investigations to date [24,28], main sources of acoustic emission are known to be microcracks, loss of cohesion, macrocracks, friction between the surfaces of macrocracks and, lastly, disintegration of material. Single AE signals and their series are also emitted in the elastic range and indicate certain local instabilities before global instability of the whole mass of the tested material develops [24]. It is here worth emphasizing that the process of failure of brittle materials such as rocks is scale-independent [24, 30] which means that the same mechanical process takes place in a small sample (in the laboratory), in a situation with moderate dimensions (mining subsidence areas) as well as during an earthquake where enormous dimensions are involved. That is why laboratory tests can provide conclusions applicable in situations of different scales.

Most commonly used parameter in the AE method to study deformation processes is the number of impulses $N/\Delta t$ per unit of time. Dependence of this number on the duration of loading is a characteristic feature of a given brittle material, its structure, behaviour etc. Another basic parameter of the AE method is the energy of signal, What is measured is the sum of signal energies in unit time: RMS. This parameter confirms information collected from the number of impulses and shows how abrupt the studied process of mechanical failure is.

The collected data concerning these parameters have shown that the process of static deformation of uniaxially compressed brittle material cylindrical samples can be divided into a number of stages each of which corresponds to a specific structural state of the material subject to cracking and failure (cf. Fig.9).

STAGE I – fixing of a specimen in the testing machine

At relatively low stresses a considerable activity of AE is present, both RMS and $N/\Delta t$. Load-displacement relationship is nonlinear (for specimen BV/6 $t = 0 - 2$ min). Small cracks appear near the end of cylinders.

STAGE II – generation of microcracks

Both RMS ($t = 2 - 7$ min) and $N/\Delta t$ become less active; and cracks continue to develop.

STAGE III – generation of macrocracks

Energy impulses RMS tend to "explode" ($t = 7-12$ min) accompanied by further instantaneous emission $N/\Delta t$. Cracks and slip lines become visible. Stable propagation of cracks continues.

STAGE IV – primary failure

Acoustic activity $N/\Delta t$ and RMS is again strong ($t = 12 - 14.5$ min) Liiders – Hartman – Cherenkov lines appear. Cracks begin to propagate in an unstable manner. An interval of time elapsing between the commencement of primary failure (so-called precursor) and complete disintegration of the specimen is usually characterized by lower activity of $N/\Delta t$.

STAGE V – failure

Immediately prior to and during the ultimate failure both the number of impulses and their energy (RMS) suddenly increase.

Completely different character of the later stages of the deformation process is observed during dynamic compression of cylinders in the Hopkinson bar. Slender specimens ($s \geq 1$) undergo, apart from primary longitudinal cracks, also secondary transversal cracks caused by tensile stresses generated in the stress wave process occuring in long specimens. These zones appear near the areas of load application and grow together with increasing strain rates to contribute to a complete disintegration of the specimen. Short specimens ($s \leq 1$) undergo longitudinal cracking only: for $s = 0.5$ across the whole length irrespective of the load level, for $s = 1$ at some parts depending on the load intensity (similarly as in the case $s \geq 1.5$).

5. COMPARISON OF RESULTS

The described experiments have enabled the new brittle photoelastic material to be studied in compression within two ranges of strain rates: low (static tests) and high (dynamic tests). The material is found to be strain rate sensitive both in the elastic range (considerable increase in Young's

modulus) and in the plastic range (different dynamic characteristics). Excellent exposition of the situation is given in Fig.15 in which the $\sigma - \varepsilon$ diagram is plotted for the specimens with the slenderness $s = 0.5$.

Larger elastic deformations are noticed under static than under dynamic loading. This can be explained by the fact that for low strain rates not only purely elastic but also viscoelastic strains have enough time to develop. For high strain rates the elastic strains are of almost completely instantaneous nature. Increase in strain rate is observed to increase elasticity of the material and at the same time to decrease its short-term strength (Fig.16). The latter fact is explained by a ductile-brittle character of failure under static load and a brittle one under dynamic load.

Proper selection of slendernesses of specimens to obtain a uniaxial stress state has been confirmed:

- $s = 2$ in static tests; effects of frictional contact are eliminated in the middle part of specimen.
- $s = 0.5$ in dynamic tests; wave propagation effects are disposed of.

Due to the transparency of the model material a full visualization of current states has been possible. In particular:

- crack propagation,
- defect and fracture mechanisms,
- plastic flow lines,
- effects of frictional forces,
- stress concentrations near cracks.

Geometry of specimens has also been found to have considerable effect on the stress-strain relationships and the fracture mechanisms. In dynamic tests the $\sigma - \varepsilon$ curves turned out to be different for slender specimens ($s > 1$) from those for short specimens ($s \leq 1$). Effects of slenderness in the static tests were observed not earlier than on the post-critical branch of the $\sigma - \varepsilon$ curve (after the short-term strength has been reached); the shape of this branch strongly depends on the failure mechanism of the specimen. In the dynamic tests defects and fracture are accompanied by longitudinal and transversal cracks, the latter being present only in the specimens with the slenderness $s > 1$. Regions of defects and failure originate from the loaded end of specimen and, together with the intensity of defects, depend on the loading rate. For specimens with $s = 0.5$ failure occurs along the whole height. In the static tests, compression failure prevails for $s > 1$, skew shears and longitudinal splitting are present for $s = 1$, cracks are accompanied by surface spalling for $s = 0.5$. Each of the above mechanisms is characterized

by a different post-critical $\sigma - \varepsilon$ branch. Fragmentation in the case of static load is finer than in the dynamic case.

ACKNOWLEDGEMENT

The authors wish to express their thanks for the cooperation and valuable discussions to E. STEWARSKI from the Geomechanics Institute of the Mining Academy of Cracow, M. KIERSNOWSKI from the Section of Nondestructive Testing of IFTR PAS, S.P. GADAJ and E. PIECZYSKA from the Section of Boundary Layer of Solid Bodies of IFTR PAS.

Test results were prepared within the Research Programme No.3 1014 9101 "Thermomechanics of defects and phase changes in the materials" sponsored by the KBN Research Committee, Poland.

REFERENCES

1. M.WOLNA, L.KRUSZKA, *Brittle photoelastic materials in the investigations of stress and strain states* [in Polish], IFTR PAS Reports 22, 1991.
2. J.GUSTKIEWICZ, *On inaccuracies in the uniaxial tests on rocks* [in Polish], Arch. Górnictwa, **20**, 1, 17–39, 1975.
3. J.KLEPACZKO, *The modified Hopkinson bar* [in Polish], Mech. Teoret. i Stos., **9**, 4, 479–497, 1971.
4. C.J.MAIDEN, S.J.GREEN, *Compressive strain-rate tests on six selected materials at strain rates from* 10^{-3} *to* 10^{4} *in/in/sec*, J. Appl. Mech., September, 496–504, 1966.
5. S.C.CHOU, K.D.ROBERTSON, J.H.RAINEY, *The effect of strain rate and heat developed during deformation on the stress-strain curve of plastics*, Exp. Mech., **13**, 10, 422–432, 1973.
6. J.KLEPACZKO, *On the rate sensitivity of coal*, Rozpr. Inż., **31**, 3, 341–360, 1983.
7. J.BUCHAR, F.DUSEK, *The influence of loading rate on mechanical properties of rocks*, Arch. Górnictwa, **20**, 2, 245–259, 1975.
8. D.KRZYSZTON, T.MIKOS, E.STEWARSKI, *Investigation of rock sample dynamic properties on the Hopkinson modified bar device*, Arch. Górnictwa, **31**, 4, 661–688, 1986.
9. B.LUNDBERG, *A split Hopkinson bar study of energy absorption in dynamic rock fragmentation*, Int. J. Rock Mech. Min. Sci., **13**, 187–197, 1976.
10. R.J.CHRISTENSEN, S.R.SWANSON, W.S.BROWN, *Split Hopkinson bar tests on rock under confining pressure*, Exp. Mech., **12**, 1, 500, 1972.

11. V.S.LINDHOLM, L.H.YEAHLEY, A.NAGY, *The dynamic strength and fracture properties of Drosser basalt*, Int. J. Rock Mech. Min. Sci., **11**, 181–191, 1974.

12. L.E.MALVERN, D.A.JENKINS, T.TANG, C.A.ROSS, *Compressive split Hopkinson bar testing of concrete*, Proc. the Int. Symp. on Intense Dynamic Loading and Its Effects, Science Press, Beijing, China 1986, 726–731.

13. J.BHARGAVA, A.REHNSTROM, *Dynamic strength of polymer modified and fiber-reinforced concretes*, Cement and Concrete Research, 7, 198–208, 1977.

14. L.KRUSZKA, W.K.NOWACKI, M.WOLNA, *Static and dynamic tests on brittle photoelastic material* [in Polish], IFTR Reports 3, 1992.

15. J. BAUER, *Considerations on the design of a stiff testing machine*, Studia Geotechnica et Mechanica, 4, 3-4, 3–14, 1982.

16. A.C.NELSON, C.Y.WANG, *Non-destructive observation of internal cracks in stressed rocks*, Int. J. Rock. Mech. Min. Sci., **14**, 103–107, 1977.

17. E.HOEK, *Rock mechanics laboratory testing in the context of a consulting engineering organisation*, Int. J. Rock Mech. Min. Sci., **14**, 93–101, 1977.

18. J.ZAWADA, *Experimental analysis of a rock block compressed between two plates*, Rozpr. Inż., **28**, 1, 129–137, 1980.

19. S.HARPALIANI, *Specimen preparation for testing coal properties*, Int. J. Rock Mech. Min. Sci., **25**, 327–330, 1988.

20. L.KRUSZKA, W.K.NOWACKI, M.WOLNA, *Experimental investigations of fracture mechanisms in brittle photoelastic materials*,In: Proc. VII European Conference on Fracture, Budapest 1988, vol. 2, 523–525.

21. G.R.HOLZHAUSEN, A.H.JOHNSON, *Analyses of longitudinal splitting of uniaxially compressed rock cylinders*, Int. J. Rock Mech. Min. Sci., **16**, 163–177, 1979.

22. C.H.SCHOLZ, *Experimental study of the fracturing process in brittle rock*, J. Geophys. Res., **73**, 1447–1454, 1968.

23. H.E.READ, G.A.HEGEMIER, *Strain softening of rock, soil and concrete – a review article*, Mech. Mat., 3, 271–294, 1984.

24. A.JAROSZEWSKA, *Study of the effects of deformation stages in certain rocks on the parameters of acoustic emission* [in Polish], Technika Poszukiwań Geologicznych, 1(121), 28–33, 1986.

25. P.PATAS, *Properties of shale concrete in bioaxial compression* [in Polish], Arch. Inżyn. Lądowej, **19**, 549–565, 1973.

26. P.LOBODA, M.SZOSTEK, *Size effects of a sample on the strength of mortars* [in Polish], Inż. i Bud., 1, 1981 and authors' reply in: Inż. i Bud., 8–9, 219–220, 1982.

27. S.MIASTKOWSKI, *Mechanical properties of materials under tension and compression* [in Polish], IFTR PAS Reports 43, 1976.

28. M.A.HAMSTAD, *A review: acoustic emission, a tool for composite materials studies*, Exp. Mech., 3, 7–13, 1986.

29. B.T.BRADY, *An investigation of the scale invariant properties of failure*, Int. J. Rock Mech. Min. Sci. and Geomech. Abstr., 14, 1977.

30. M.C.REYMOND, J.BILLAUD, *Emission acoustique dans les rockes calcaires a differentes echelles*, Revue d'Acoustique, 52, 1980.

31. C.CAZENEUVE, J.C.MAILE, *Etude du comportement da composites á fibres de carbonne sous différentes vitesses de déformation*, J. Physique, 46, 8, 551–556, 1985.

MILITARY TECHNICAL ACADEMY, WARSZAWA
and
POLISH ACADEMY OF SCIENCES
INSTITUTE OF FUNDAMENTAL TECHNOLOGICAL RESEARCH.

Received March 14, 1992.